Knot probability of polygons subjected to a force: a Monte Carlo study

2008 J. Phys. A: Math. Theor. 41 025003

(http://iopscience.iop.org/1751-8121/41/2/025003)

IOP PUBLISHING JOURNAL OF PHYSICS A: MATHEMATICAL AND THEORETICAL

J. Phys. A: Math. Theor. **41** (2008) 025003 (13pp) doi:10.1088/1751-8113/41/2/025003

Knot probability of polygons subjected to a force: a Monte Carlo study

E J Janse van Rensburg[1], E Orlandini[2], M C Tesi[3] and S G Whittington[4]

[1] Department of Mathematics and Statistics, York University, Toronto M3J 1P3, Canada
[2] Dipartimento di Fisica, CNR-INFM, and Sezione INFN, Università di Padova, Padova, Italy
[3] Dipartimento di Matematica, Università di Bologna, Bologna, Italy
[4] Department of Chemistry, University of Toronto, Toronto M5S 3H6, Canada

E-mail: orlandini@pd.infn.it

Received 13 September 2007, in final form 15 November 2007
Published 19 December 2007
Online at stacks.iop.org/JPhysA/41/025003

Abstract

We use Monte Carlo methods to study the knot probability of lattice polygons on the cubic lattice in the presence of an external force f. The force is coupled to the span of the polygons along a lattice direction, say the z-direction. If the force is negative polygons are squeezed (the compressive regime), while positive forces tend to stretch the polygons along the z-direction (the tensile regime). For sufficiently large positive forces we verify that the Pincus scaling law in the force–extension curve holds. At a fixed number of edges n the knot probability is a decreasing function of the force. For a fixed force the knot probability approaches unity as $1 - \exp(-\alpha_0(f)n + o(n))$, where $\alpha_0(f)$ is positive and a decreasing function of f. We also examine the average of the absolute value of the writhe and we verify the square root growth law (known for $f = 0$) for all values of f.

PACS numbers: 02.10.Kn, 36.20.Ey, 05.70.Jk, 87.15.Aa

(Some figures in this article are in colour only in the electronic version)

1. Introduction

There is considerable recent interest in the response of polymers and filaments to an applied force. Experiments are now possible, for instance using atomic force microscopy [2, 3, 8] or optical tweezers [1, 19], where an individual polymer can be elongated and the stress–strain curve investigated [2].

In this paper the knot probability of a ring polymer subjected to a compressive or elongational force is examined. The knot type of the polymer is not fixed; this corresponds to a situation where an enzyme (for example topoisomerase acting on DNA) can allow strand passage. This establishes at a fixed force an equilibrium distribution of knotted conformations.

We model ring polymers by cubic lattice polygons. The cubic lattice $\mathbb{Z}^3$ consists of integer points in $\mathbb{R}^3$, and of edges which are unit length line segments between pairs of vertices which are unit distance apart in $\mathbb{R}^3$. A *polygon* is an embedding of a simple closed curve in $\mathbb{Z}^3$. We shall write p_n for the number of (undirected, unrooted) polygons with n edges, so that $p_4 = 3$, $p_6 = 22$, etc. For a given polygon ω with vertices $\omega_1, \omega_2, \ldots$ the span along the z-direction (Z-span) is defined as

$$s(\omega) = \max_{ij} |z(\omega_i) - z(\omega_j)|, \tag{1}$$

where $z(\omega_i)$ is the third coordinate of the ith vertex ω_i of the polygon.

Let $p_n(s)$ be the number of n-edge polygons with Z-span s. In the *constant force ensemble* (or stress ensemble) the equilibrium properties of the system are described by the partition function

$$Z_n(\tilde{f}) = \sum_s p_n(s)\, \mathrm{e}^{\tilde{f}s/k_BT} \tag{2}$$

where $\tilde{f}$ is the applied force. We consider forces in units of inverse length by defining $f = \tilde{f}/k_BT$. If $f = 0$ we have $Z_n(0) = p_n$. For compressive forces ($f < 0$) the polygons are squeezed along the z-direction, while for $f > 0$ (tensile forces) polygons elongated along the z-direction are more favorable.

It is straightforward to prove, using concatenation arguments and subadditivity, that the limiting free energy

$$\lim_{n\to\infty} n^{-1} \log Z_n(f) \equiv \mathcal{F}(f) \tag{3}$$

exists. For $f = 0$ it is known that sufficiently long polygons are almost surely knotted [17, 18]. This result is based on a pattern theorem for polygons.

A pattern theorem has recently been proved [11] for polygons subject to a sufficiently large tensile force which implies that the probability $P_n(f)$ that a polygon with n edges, subject to a force f, is knotted behaves as

$$P_n(f) = 1 - \mathrm{e}^{-\alpha_0(f)n + o(n)} \tag{4}$$

for f sufficiently large and positive, as well as for $f = 0$. At the moment we do not know of any rigorous results about the knot probability in either the compressive or weak tensile regimes.

We also consider a model where the compressive force is applied to two fixed vertices of the n-edge polygon, $n/2$ edges apart. The appropriate partition function is then

$$\bar{Z}_n(f) = \sum_d p_n(d)\, \mathrm{e}^{\tilde{f}d/k_BT}, \tag{5}$$

where the force is now coupled to the projection d on the z-coordinate of the line between two fixed vertices of the polygon, $n/2$ edges apart. One can imagine this model being relevant to an AFM experiment, where the size L of the AFM tip is small relative to the persistence length L_p of the ring polymer itself. If $L \gg L_p$ the compressive regime can be well described by the partition function given in (2).

We will refer to the models described by (2) and (5) as model 1 and model 2 respectively.

2. Numerical results

Lattice polygons with fixed number of vertices can be sampled efficiently by Monte Carlo methods based on the pivot algorithm for polygons [13]. Although the pivot algorithm works

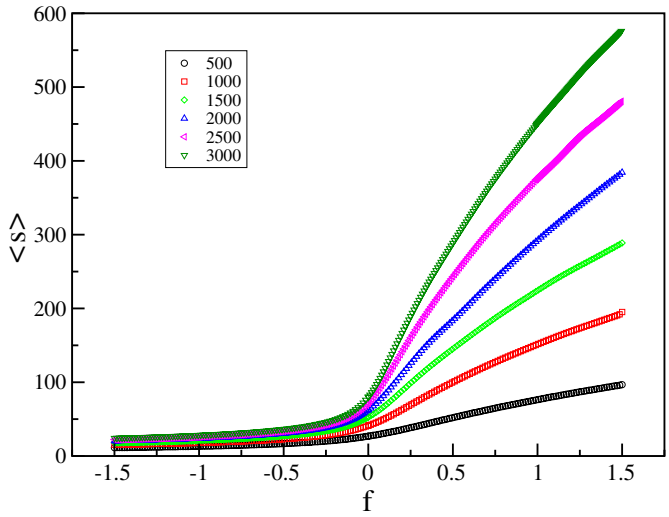

Figure 1. Average span $\langle s \rangle$ along the force direction as a function of the force f for different n values.

well for $f = 0$, at large values of f it may suffer from quasi-ergodic problems which would make the sampling less efficient. We overcome this difficulty by using a multiple Markov chain (MMC) implementation of the above algorithm [5, 6]. The idea is to run a set of Markov chains in parallel (at a fixed set of f values) and swap configurations between the individual Markov chains. For details see Tesi *et al* [22] and Orlandini *et al* [15].

We carried out simulations by considering up to 40 Markov chains in parallel and by sampling configurations every m attempted pivot moves. The value of m which we used increased with the size n of the polygon and ranged from 2000 (for $n = 500$) up to 12 000 (for $n = 3000$). The data were then analyzed by using standard techniques to estimate the autocorrelation times and the statistical confidence intervals [14]. In addition, we have used the multi-histogram reweighting technique to estimate the density of states $p_n(s)$ and from that the partition function $Z_n(f)$ [20]. Given an estimate of $Z_n(f)$ all the interesting averages are easily obtained.

2.1. Stretching regimes

Since the force is applied along the z-direction the order parameter of the model is the average extension along the stretching force direction i.e. the average Z-span

$$\langle s \rangle = \frac{\partial}{\partial f} \log Z_n(f). \tag{6}$$

Figure 1 shows the f dependence of the average value of s, for different values of n. For fixed n, $\langle s \rangle$ is a monotonic non-decreasing function of the applied force. For tensile forces ($f > 0$) the polygons tend to be stretched and the force–extension curve shown in figure 1 can be explained according to the Pincus theory of stretched polymers in good solvents [4, 16]. This theory identifies two characteristic length scales in the problem: the average radius of gyration $R \propto n^{\nu}$ where ν is the metric exponent, and the tensile screening length $\xi = 1/f$. The cases of weak and strong forces correspond, respectively, to the conditions

$R/\xi \ll 1$ and $R/\xi \gg 1$. The scaling assumption consists in assuming that, for arbitrary positive f, the extension along the stretching direction $\langle s \rangle$ can be written as

$$\langle s \rangle = R\Phi(R/\xi), \tag{7}$$

where $\Phi(x)$ is a dimensionless scaling function.

According to Pincus [16] one should then distinguish three stretching regimes.

- *Weak force regime*. For small forces one should expect a linear increase in the extension s as f increases (Hooke's law). Thus, $\Phi(x \to 0) \sim x$ and

$$\langle s \rangle \propto R^2 f = n^{2\nu} f. \tag{8}$$

  Note that for chains with no excluded volume interaction (ideal chains) $\nu = 1/2$ and $\langle s \rangle$ is linear in n at low forces. For self-avoiding walks $\nu \approx 0.588$ and the average extension is a nonlinear function of n. In the ideal case, the force is transmitted along the backbone while for self-avoiding walks the transmission is also through contacts between pairs of monomers due to excluded volume interactions. Note that scaling (8) implies

$$f = K\langle s \rangle, \tag{9}$$

  i.e. the force–extension curve obeys the Hooke law with elastic constant K that decreases as $n^{-2\nu}$.
- *Intermediate force regime*. In the strongly stretched regime, which arises for intermediate forces, the value of $\langle s \rangle$ can be obtained according to a 'blob' interpretation in which the chain can be broken into a sequence of aligned (along the force direction) tensile blobs whose size is $\xi \sim f^{-1} = (\tilde{f}/k_B T)^{-1}$. The blobs do not interact with one another and the monomers contained in each blob behave as unperturbed self-avoiding walks. That is $\xi \sim n_b^{\nu}$, where n_b is the number of monomers in each blob. The linear extension of the chain is then given by $\langle s \rangle \sim \xi n/n_b \sim n f^{1/\nu - 1} \sim n f^{2/3}$, where we have used the Flory value of the exponent $\nu = 3/5$. This is the so-called Pincus regime. In this case

$$f = K\langle s \rangle^{3/2} \tag{10}$$

  with $K \sim n^{-3/2}$. It is important to note that this argument is valid only in the limit $n \gg \xi^{1/\nu} \gg 1$, which may not be satisfied for a stiff polymer or a flexible one with small n.
- *Strong force regime*. For extremely large forces excluded volume effects become irrelevant since the bonds of the polymer are fully aligned along the stretching direction and monomers do not interact with one another. In this case $\langle s \rangle$ becomes comparable to n and the force–extension relation for the chain is dominated by the bonding potential between consecutive monomers. As a result, the force–extension curve would be model dependent.

Figure 2 shows $\langle s \rangle / n^{\nu}$ versus $f n^{\nu}$ where $\nu = \nu_{\text{saw}} \simeq 0.588$ for positive forces. As n increases the data collapse onto a single curve. For small positive values of f the behavior is linear as suggested by the dashed straight line. For larger values of f the curves collapse by plotting $\langle s \rangle / n$ as a function of f (see figure 3). The dashed curve represents the best fit of the data for $n = 3000$ to the function An^c. The estimate $c \approx 0.64$ is quite close to the value $2/3$ characterizing the Pincus regime. Our values of f are not large enough to see the non-universal regime. Note that longer polygons reach the scaling regime at weaker forces. Indeed, the rigidity of a long chain is smaller than that of short chains and this makes longer polygons more easily deformed.

In the Pincus regime the argument used by Pincus is that the blobs are not internally deformed by the force, but the sequence of blobs is elongated along the direction of the force.

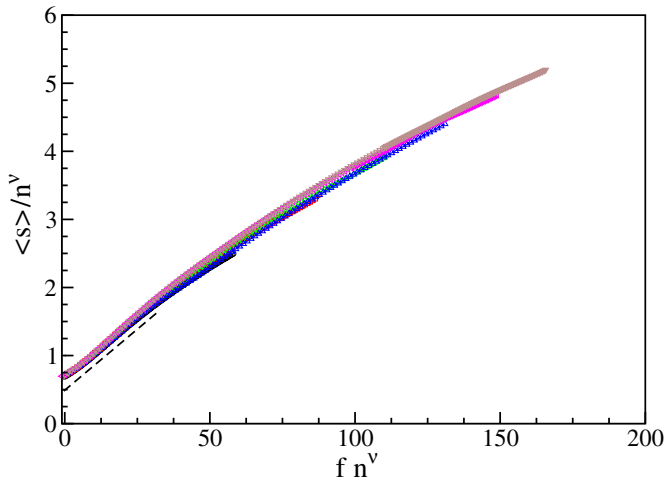

Figure 2. Same data as in the previous figure but now the average span along z is divided by n^{ν} and the force is multiplied by n^{ν} with $\nu = 0.588$ being the metric exponent of self-avoiding walks in $d = 3$. The data are for positive forces. The dashed straight line indicates the linear behavior for small values of f.

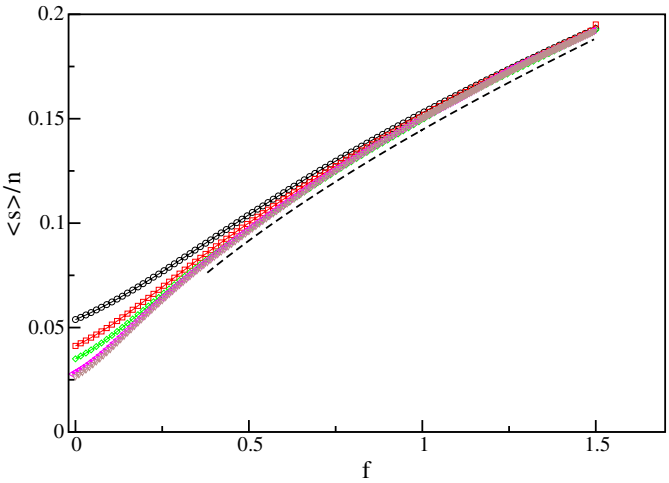

Figure 3. Same data of the previous figure but now the span along z is divided by n. The dashed curve corresponds to the fit $An^{0.64}$ for the $n = 3000$ case. This gives the Pincus regime.

This implies that the blobs behave more or less independently in this regime. Since each blob can contain a knot with positive probability this independence implies that an infinitely long chain will be knotted with probability 1 and the exponential constant $\alpha_0(f)$ should be roughly independent of f in this regime [7].

In figure 4 (inset) we plot the component of the root mean square radius of gyration along the force direction, $\langle R_f \rangle$, as a function f. Different curves correspond to different values of n. If the data are scaled by following (8), they all collapse nicely onto a single curve for all the positive forces considered (see the main plot of figure 4). This is expected since in the tensile regime the component $\langle R_f \rangle$ would be the dominant one. If we consider instead the total root

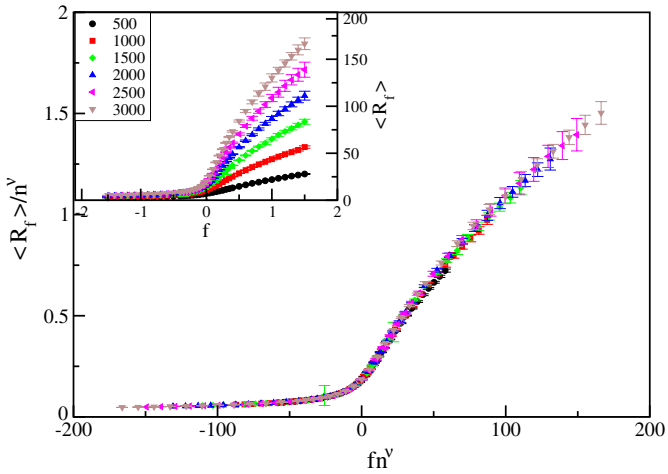

Figure 4. The raw data $\langle R_f \rangle$ versus f shown in the inset are rescaled in the main plot as $\langle R_f \rangle / n^\nu$ versus fn^ν to show that the Pincus scaling law holds also for the projection of the mean square root radius of gyration on the direction of the force.

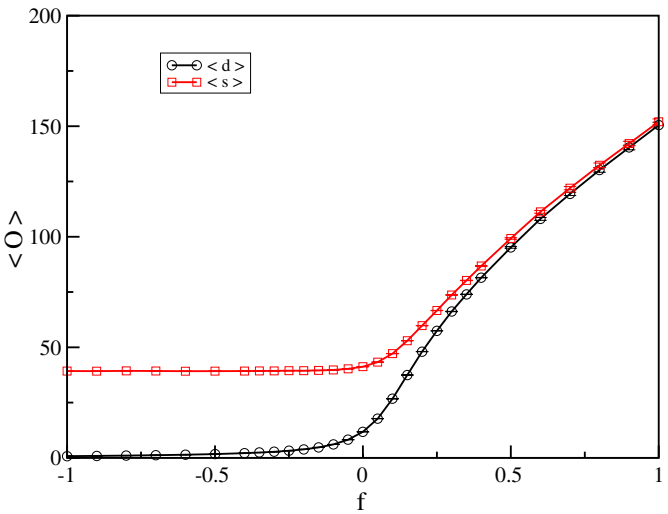

Figure 5. Comparison between the variable d conjugate to the force in model 2 and the average span along the direction of the force. The case displayed corresponds to polygons with $n = 1000$ steps.

mean square radius of gyration the collapse is not as good as for its component along the force direction.

While the metric properties of model 1 and model 2 are expected to be similar in the tensile regime they differ in the compressive regime. Indeed, in model 2 negative forces would bring the two opposite (along the backbone) edges close together along the z-coordinate leaving the span along the force direction close to the natural span i.e. the span for $f = 0$ (see figure 5).

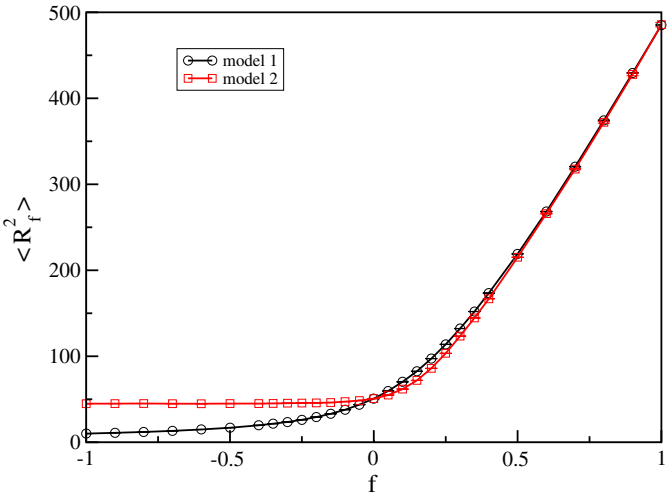

Figure 6. Component of the mean square radius of gyration along the force direction for the two different models and for $n = 500$. Note that for model 2 this quantity is almost constant (and equal to its value for $f = 0$) for negative values of f (squeezing regime), while for f sufficiently high (stretching regime) the two models display the same behavior as expected.

A further indication of the difference between the two models in the compressive regime is given by comparing the components along the force direction of the mean root squared radius of gyration (see figure 6) in the two cases: in model 1 this quantity is still decreasing as the force becomes more and more negative while it remains constant for model 2.

2.2. *Knot probability*

Knots in polygons can be detected by computing the value of the Alexander polynomial $\Delta(t)$ at $t = -1$ (see, for example, the work of Volodogskii *et al* [23] and Janse van Rensburg [10]). If $|\Delta(-1)| \neq 1$ then the polygon is a knot. Otherwise we assume that it is the unknot. In fact the Alexander polynomial is not a perfect invariant, and is unable to distinguish every knot type. For instance, the prime knot 8_{11} has the same Alexander polynomial as the composite knot $3_1\#6_1$, and 8_{15} has the same Alexander polynomial as $3_1\#7_2$. To help to distinguish pairs of knots we have also computed $|\Delta(-2)|$. In figures 7 and 8, we compare the data analyzed using time series methods with the curve estimated by the multi-histogram method. The multi-histogram seems to work quite well and has the advantage of giving continuous curves in f.

In figure 9, we show the knot probability as a function of f for different values of n.

For each fixed n the knot probability decreases rapidly as the tensile force (f positive) increases while it increases (but slowly) in the compressive regime. For a fixed value of f we confirm the exponential decay of the unknotting probability i.e.

$$P_n^0(f) = \mathrm{e}^{-\alpha_0(f)n+o(n)}. \tag{11}$$

This result is known rigorously for $f = 0$ [18] and also for f sufficiently large and positive [11]. However, there are no corresponding rigorous results for $f < 0$ or for f positive and small.

In figure 10, the unknot probability as a function of n is reported for some values of the force. A log–linear fit of such curves gives an estimate of $\alpha_0(f)$ for different values of f.

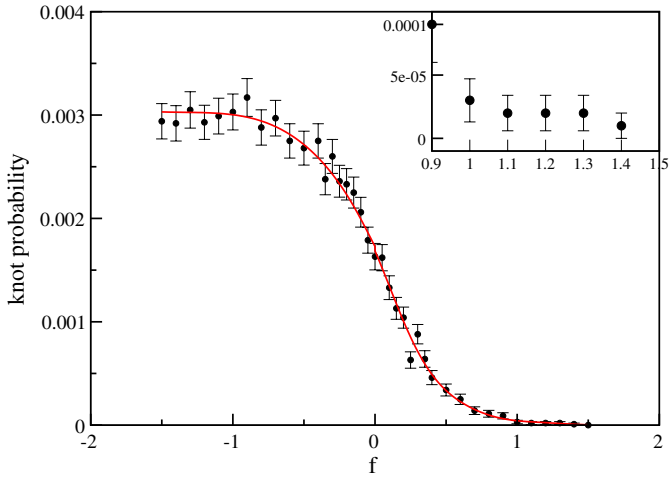

Figure 7. Knot probability as a function of the force f for $n = 500$: the circles correspond to the direct estimates coming from the data (the errors are obtained by performing the time correlation function estimate), while the continuous curve corresponds to the multi-histogram method. The inset shows an enlargement of the main plot for $f \geqslant 1$.

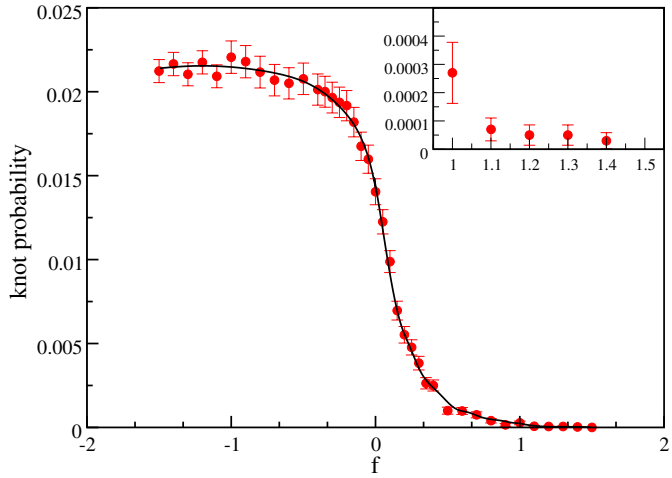

Figure 8. Knot probability as a function of the force f for $n = 3000$: the circles correspond to the direct estimates coming from the data (the errors are obtained by performing the usual time correlation function estimate), while the continuous curve corresponds to the multi-histogram method. The inset shows an enlargement of the main plot for $f \geqslant 1$.

In figure 11, these estimates are plotted as a function of f. We note that $\alpha_0(f)$ is small and decreases as f increases. The values are much smaller for f positive than for f negative. For $f = 0$ the estimate agrees within the error bars with the estimate of Janse van Rensburg [10]. For f greater than 1, $\alpha_0(f)$ is roughly constant, though not zero. This is consistent with the expectation that in the Pincus regime the polymer can be described by non-interacting blobs [7].

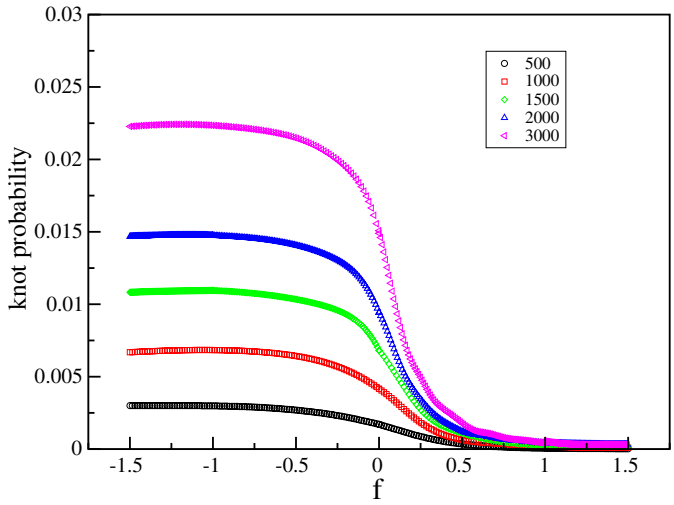

Figure 9. Knot probability as a function of the force f for different n values.

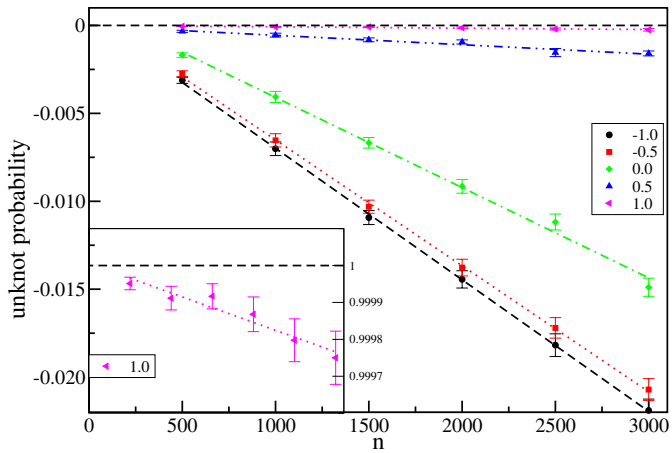

Figure 10. Log–linear plots of the unknot probability as a function of n. Different curves correspond to different values of the force (see labels). By fitting each curve with the exponential behavior of equation (11) we get estimates of $\alpha_0(f)$. The inset shows an enlargement around 1 for the curve $f = 1.0$.

When we compare the knot probabilities for model 1 and model 2 (see figure 12) we note that they are very similar for $f \geqslant 0$ while for $f < 0$ the knot probability for model 1 is larger than for model 2. This is related to the fact that, for model 1, in the compressive regime the polygon is effectively confined to a slab leading to a larger knot probability [21]. Moreover, since in model 2 the polygons are not globally compressed the knot probability is not seriously affected and remains roughly constant for all the negative values of f considered.

This feature holds for all the values of n considered here (see figure 13) and gives rise to values of $\alpha_0(f)$ that, for model 2, are roughly independent of the strength of the compressive force.

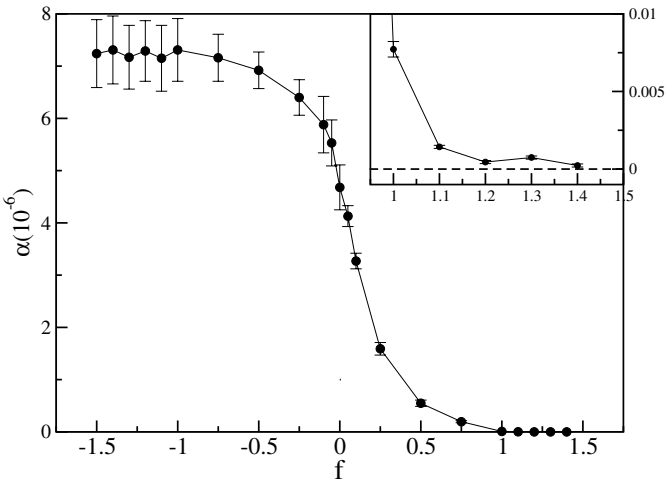

Figure 11. Estimates of the unknotting exponent as a function of the force. The inset shows an enlargement of the region $f \geqslant 1$.

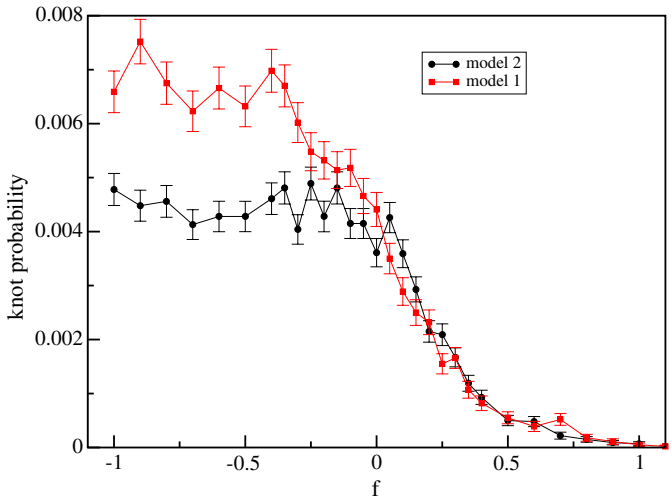

Figure 12. Comparing the knot probability as a function of f of the two models. The data correspond to polygons of $n = 1000$ steps.

Given that a polygon subjected to a compressive or tensile force is knotted it is interesting to investigate the relative amounts of different knot types (i.e. the knot spectrum as a function of f). In order to estimate the knot spectrum we have sampled $\sim 5 \times 10^5$ polygons with $n = 6000$ steps for some values of the force. The knot type of each configuration has been detected by computing the HOMFLY polynomial. The relative frequencies of the first simple knots are reported in table 1.

It is clear that as the tensile force increases the proportion of complex knots decreases and simple knots dominate. For compressive forces the proportion of trefoils observed was relatively constant, and roughly equal to the proportion when no force is applied.

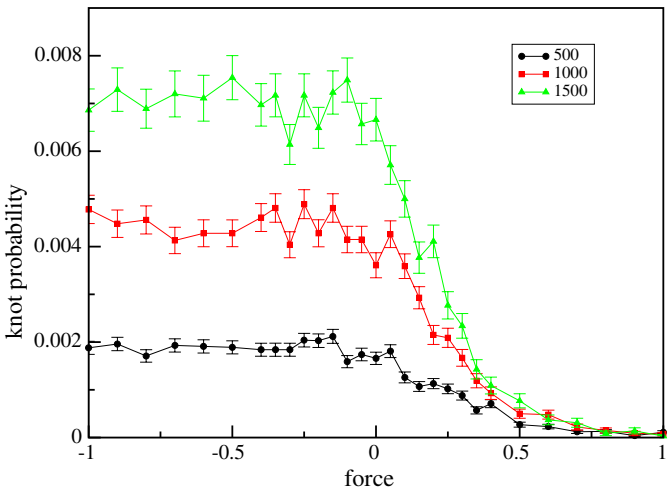

Figure 13. Knot probability as a function of f for model 2. The three curves correspond to three different values of n. Note that in the compressive regime the knot probability is almost independent of f.

Table 1. Percentage of the fraction of the occurrence of the simplest knot types (columns 4–9) within the subset of knotted polygons (third column) with $n = 6000$.

	No. of configurations	No. of knots	3_1	4_1	5_1	5_2	$3_1\#3_1$	Others
−2.0	315 760	12 811	92.60 ± 0.23	4.39 ± 0.18	0.43 ± 0.06	0.60 ± 0.07	1.64 ± 0.11	0.34 ± 0.03
−1.0	315 548	10 647	92.76 ± 0.25	4.48 ± 0.20	0.35 ± 0.06	0.70 ± 0.08	1.16 ± 0.10	0.55 ± 0.04
0.0	315 541	9 887	92.66 ± 0.26	4.56 ± 0.21	0.55 ± 0.07	0.57 ± 0.08	1.37 ± 0.12	0.29 ± 0.04
0.1	315 866	7 163	94.44 ± 0.27	3.56 ± 0.22	0.19 ± 0.05	0.47 ± 0.08	1.12 ± 0.12	0.20 ± 0.05
0.5	361 414	898	98.66 ± 0.38	1.34 ± 0.39	0.00	0.00	0.00	0.00
1.0	257 258	78	100.0	0.00	0.00	0.00	0.00	0.00

In addition to the topological entanglement complexity we have checked how the geometrical entanglement complexity can be affected by a force. One useful measure of geometrical entanglement complexity is the *writhe*. Consider a simple closed curve and project this onto a plane in direction $\hat{x}$. The projected curve will have a set of (transverse) crossings which we label $i = 1, 2, \ldots$, where the ith crossing has crossing number $\sigma_i = \pm 1$. Form the sum of these crossing numbers and average over all projection directions, $\hat{x}$. This is the writhe, Wr, of the curve. For lattice polygons this can be conveniently computed using a result of Lacher and Sumners [12]. Because the writhe can be positive or negative we concentrate on the absolute value $|Wr|$. For polygons in the absence of a force it is known rigorously [9] that $\langle |Wr| \rangle \geqslant A\sqrt{n}$ for some positive constant A and for n large, where the angular brackets denote expectation for a fixed value of n. In figure 14 we show the average of $|Wr|$ as a function of f for model 1 (see the inset). The data collapse onto a single curve if $\langle |Wr| \rangle$ is rescaled by $\sqrt{n}$ (see the main plot in figure 14).

For $f = 0$ and for f sufficiently large and positive a pattern theorem together with a coin tossing argument shows that

$$\langle |Wr| \rangle \geqslant A\sqrt{n} \tag{12}$$

for some $A > 0$ and for n sufficiently large [11]. Our numerical results suggest that this bound might be best possible and that it applies for all values of f.

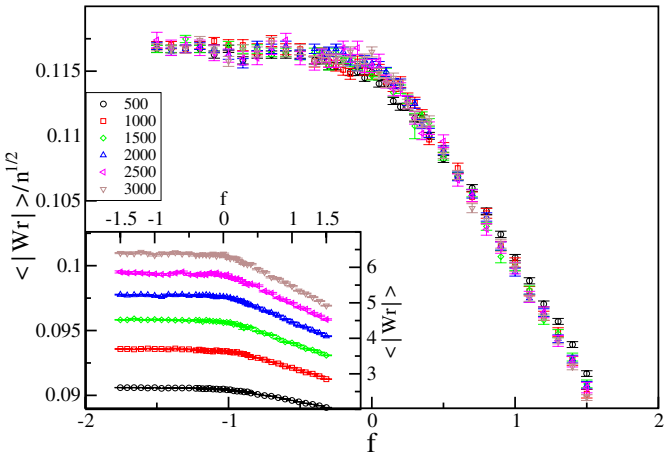

Figure 14. The average of the absolute value of the writhe $\langle |Wr| \rangle$ versus f is shown in the inset for different values of n. In the main figure, these data have been rescaled by $n^{1/2}$ to show that the same power law behavior holds for all the values of f considered.

3. Summary and discussion

We have used Monte Carlo methods to investigate the properties of lattice polygons in three dimensions under the influence of a tensile and a compressive force. The data for the span of the polygons in the direction of the applied force show clear evidence of different scaling behavior in the weakly and strongly stretched regimes, consistent with the scaling theory of Pincus.

We have examined the knot probability as a function of force and find that the probability of being knotted goes to unity exponentially rapidly as the size of the polygon goes to infinity, for all forces studied. This agrees with rigorous results both for zero force and for very strong tensile forces, though there are no corresponding rigorous results for compressive forces or for weak tensile forces. We have also examined the distribution of knot types at different forces. The knot distribution is not sensitive to the force in the compressive regime but more complex knots become rarer at large tensile forces.

We have also examined the writhe, as a measure of geometric entanglement complexity and we find that the mean of the absolute value of the writhe scales like $\sqrt{n}$ at all forces examined.

Acknowledgments

EJJvR and SGW acknowledge support in the form of Discovery Grants from NSERC of Canada. EO was supported by a grant from MIUR-PRIN05.

References

[1] Ashkin A 1997 Optical trapping and manipulation of neutral particles using lasers *Proc. Natl Acad. Sci. USA* **94** 4853–60

[2] Bemis J E, Akhremitchev B B and Walker G C 1999 Single polymer chain elongation by atomic force microscopy *Langmuir* **15** 2799–805

[3] Bustamante C and Keller D 1995 Scanning force microscopy in biology *Phys. Today* **48** 32–8
[4] de Gennes P G 1979 *Scaling Concepts in Polymer Physics* (New York: Cornell University Press)
[5] Geyer C J 1991 Markov chain Monte Carlo maximum likelihood *Computing Science and Statistics: Proc. 23rd Symp. on the Interface* ed E M Keramidis (Fairfax Station, VA: Interface Foundation) pp 156–63
[6] Geyer C J and Thompson E A 1995 Annealing Markov chain Monte Carlo with applications to ancestral inference *J. Am. Stat. Assoc.* **90** 909–20
[7] Grosberg A 2007 private communication
[8] Hansma H G 1996 Atomic force microscopy of biomolecules *J. Vac. Sci. Technol.* B **14** 1390–5
[9] Janse van Rensburg E J, Orlandini E, Sumners D W, Tesi M C and Whittington S G 1993 The writhe of a self-avoiding polygon *J. Phys. A: Math. Gen.* **26** L981–6
[10] Janse van Rensburg E J 2002 The probability of knotting in lattice polygons *Physical Knots: Knotting, Linking, and Folding Geometric Objects in R^3 (Contemporary Mathematics* vol 304) ed J A Calvo, K C Millett and E J Rawdon (Providence, RI: American Mathematical Society) pp 125–35
[11] Janse van Rensburg E J, Orlandini E, Tesi M C and Whittington S G 2008 Knotting in stretched polygons, *J. Phys. A: Math. Theor.* **41** 015003
[12] Lacher R C and Sumners D W 1991 Data structures and algorithms for computation of topological invariants of entanglements: link, twist and writhe *Computer Simulation of Polymers* ed R J Roe (Englewood Cliffs, NJ: Prentice-Hall) pp 365–73
[13] Madras N, Orlitsky A and Shepp L A 1990 Monte Carlo generation of self-avoiding walks with fixed endpoints and fixed length *J. Stat. Phys.* **58** 159–83
[14] Madras N and Sokal A D 1988 The pivot algorithm: a highly efficient Monte Carlo method for the self-avoiding walk *J. Stat. Phys.* **50** 109–86
[15] Orlandini E, Tesi M C, Janse van Rensburg E J and Whittington S G 1997 The shapes of self-avoiding polygons with torsion *J. Phys. A: Math. Gen.* **30** L693–8
[16] Pincus P 1976 Excluded volume effects and stretched polymer chains *Macromolecular* **9** 386–8
[17] Pippenger N 1989 Knots in random walks *Discrete Appl. Math.* **25** 273–8
[18] Sumners D W and Whittington S G 1988 Knots in self-avoiding walks *J. Phys. A: Math. Gen.* **21** 1689–94
[19] Svoboda K and Block S M 1994 Biological applications of optical forces *Ann. Rev. Biophys. Biomol. Struct.* **23** 247–85
[20] Swendsen R H and Ferrenberg A M 1989 Histogram methods for Monte Carlo data analysis *Computer Simulation Studies in Condensed Matter Physics II* ed D P Landau, K K Mon and H-B Schüttler (Heidelberg: Springer)
[21] Tesi M C, Janse van Rensburg E J, Orlandini E and Whittington S G 1994 Knot probability for lattice polygons in confined geometries *J. Phys. A: Math. Gen.* **27** 347–60
[22] Tesi M C, Janse van Rensburg E J, Orlandini E and Whittington S G 1996 Monte Carlo study of the interacting self-avoiding walk model in three dimensions *J. Stat. Phys.* **82** 155–81
[23] Vologodskii A V, Lukashin A V, Frank-Kamenetskii M D and Anshelevich V V 1974 The knot problem in statistical mechanics of polymer chains *Zh. Eksp. Teor. Fiz.* **66** 2153–63